ACS APPLIED MATERIALS & INTERFACES

Research Article

Cite This: ACS Appl. Mater. Interfaces 2018, 10, 43809−43816

www.acsami.org

High-Temperature Superconductivity in a Th−H System under Pressure Conditions

Alexander G. Kvashnin,*[,†,‡] Dmitrii V. Semenok,[†,‡] Ivan A. Kruglov,[‡,§] Izabela A. Wrona,[∥] and Artem R. Oganov*[,†,§,⊥]

[†]Skolkovo Institute of Science and Technology, Skolkovo Innovation Center, 3 Nobel Street, Moscow 143026, Russia

[‡]Moscow Institute of Physics and Technology, 9 Institutskiy Lane, Dolgoprudny 141700, Russia

[§]Dukhov Research Institute of Automatics (VNIIA), Moscow 127055, Russia

[∥]Institute of Physics, Jan Dlugosz University in Czestochowa, Armii Krajowej 13/15 Avenue, 42-200 Czestochowa, Poland

[⊥]International Center for Materials Discovery, Northwestern Polytechnical University, Xi'an 710072, China

Supporting Information

ABSTRACT: New stable phase thorium decahydride $Fm\bar{3}m$-ThH_{10}, a high-temperature superconductor with T_C up to 241 K (−32 °C), critical field H_C up to 71 T, and superconducting gap Δ_0 of 52 meV at 80−100 GPa, is predicted by evolutionary algorithm USPEX. Another phase, $P2_1/c$-ThH_7, is found to be a superconductor with T_C of 62 K. Analysis of the superconducting state was performed within Eliashberg formalism, and $H_C(T)$, $\Delta(T)$, and $T_C(P)$ functions with a jump in the specific heat at critical temperature were calculated. Several other new thorium hydrides were predicted to be stable under pressure, including ThH_3, Th_3H_{10}, ThH_4, and ThH_6. Thorium (which has s^2d^2 electronic configuration) forms high-T_C polyhydrides similar to those formed by s^2d^1 metals (Y−La−Ac). Thorium belongs to the Mg−Ca−Sc−Y−La−Ac family of elements forming high-T_C superconducting hydrides.

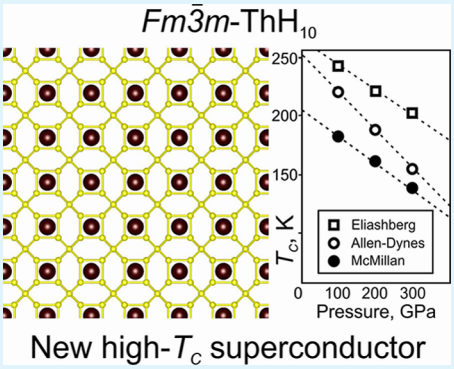

KEYWORDS: *High-T superconductivity, ThH_{10}, USPEX, DFT, Eliashberg theory, high pressure*

INTRODUCTION

Recent outstanding experimental observation of previously predicted[1] superconductivity in LaH_{10+x} by Drozdov et al.[2] and Somayazulu et al.[3] with record temperatures of 215−260 K (150−192 GPa) inspired us to search for new high-T_C superconductors in the Th−H system.

Thorium is a weakly radioactive element, its most stable isotope ^{232}Th having a half-life of 14 billion years. Thorium belongs to the actinide series, but its physical and chemical properties are mainly dictated by 6d electrons, similar to transition metals Ti, Hf, or Zr.[4] Bulk thorium has a face-centered cubic structure at normal conditions ($Fm\bar{3}m$ space group) in contrast to other elements of the actinide series[5] and is a weak conventional (phonon-mediated) type-I superconductor with T_C of 1.374 K[5,6] and critical magnetic field H_C of 15.92 mT.[7,5] Theoretical calculations of the electron−phonon coupling (EPC) have been reported to be in good agreement with experimental data.[8−10] The chemistry of actinides and their compounds is a relatively unpopular topic, but many potentially interesting materials can be discovered there. Here, we show that unique high-temperature superconductors are predicted among thorium hydrides.

Thorium reacts with hydrogen to form hydrides ThH_2 and Th_4H_{15}, the latter being the first known superconducting hydride at ambient pressure, with superconducting T_C of 7.5−8 K.[11,12] Thorium hydrides are chemically active and sensitive to air and moisture.[13] The stability and electronic properties of ThH_2 and Th_4H_{15} were studied theoretically.[14,15] Investigations of superconducting properties of hydrides and deuterides of thorium with H or D to metal atom ratios of 3.6 to 3.65 revealed the absence of the isotope effect,[16] because of either strong anharmonic contribution or non-phonon pairing mechanisms.

Recent experimental and theoretical studies show some of the hydrogen-rich hydrides forming under pressure to be high-temperature superconductors.[1,17−25] Hydrogen sulfide stands out among the rest. Using the evolutionary algorithm USPEX,[26−28] H_3S in the trigonal $R3m$ and cubic $Im\bar{3}m$ phases was predicted at high pressures (above 110 GPa) to be a high-temperature superconductor with T_C reaching 191−204 K at 200 GPa for the $Im\bar{3}m$ phase.[19] Experimental work[29] confirmed the existence of superconducting H_3S with T_C of 203 K at 155 GPa, and its crystal structure was confirmed to be $Im\bar{3}m$.[22,30] Recent predictions of high-temperature superconductivity in lanthanum, yttrium, actinium, and uranium hydrides (LaH_{10} and YH_{10},[1] AcH_{10},[31] and UH_7 and UH_9[25])

Received: September 30, 2018
Accepted: November 20, 2018
Published: December 4, 2018

DOI: 10.1021/acsami.8b17100
ACS Appl. Mater. Interfaces 2018, 10, 43809−43816

and subsequent experimental syntheses of the predicted LaH_{10+x},[32] UH_7,[25] CeH_9,[33] CrH_2, and Cr_2H_3[34] show that transition-metal hydrides are extremely promising. Thus, we decided to perform a systematic evolutionary search for new phases in the Th−H system under pressure. As we show below, one of the new hydrides is predicted to be a unique high-temperature superconductor.

COMPUTATIONAL METHODOLOGY

In this work, we used methodology similar to our previous work (e.g., ref 31). For predicting new Th−H phases, we used the evolutionary algorithm USPEX,[26−28] which is a powerful tool allowing prediction of all thermodynamically stable compounds of given elements at a certain pressure. We performed variable-composition searches in the Th−H system at pressures 0, 50, 100, 150, and 200 GPa. The first generation consisting of 120 structures was produced using random symmetric and random topological generators, whereas all subsequent generations contained 20% random structures and 80% were created using heredity, softmutation, and transmutation operators. Here, evolutionary searches were combined with structure relaxations using density functional theory (DFT)[35,36] within the Perdew−Burke−Ernzerhof functional (generalized gradient approximation)[37] and projector-augmented wave method[38,39] as implemented in the VASP code.[40−42] Kinetic energy cutoff for plane waves was 600 eV. The Brillouin zone was sampled using Γ-centered k-point meshes with a resolution of $2\pi \times 0.05$ Å^{-1}.

To determine the stability field of the predicted phases, we performed additional calculations of their enthalpies with increased precision in the considered pressure range but with a smaller pressure increment (5−10 GPa) and recalculated the thermodynamic convex hull (Maxwell construction) at each pressure. The thermodynamically stable phase has lower Gibbs free energy (or, at zero Kelvin, enthalpy) than any phase or assemblage of phases with the same net composition. Stable structures of elemental Th and H at each pressure were taken from our USPEX calculations and elsewhere.[43−45]

Calculations of superconducting T_C were carried out using the Quantum ESPRESSO (QE) package.[46] This methodology was used in our previous work.[31] Phonon frequencies and EPC coefficients were computed using density-functional perturbation theory,[47] plane-wave pseudopotential method, and the Perdew−Burke−Ernzerhof exchange-correlation functional.[37] We found that 120 Ry is a suitable cutoff energy for the plane wave basis set. Calculated electronic properties (band structure and electronic density of states [DOS]) by VASP and QE of predicted thorium hydrides demonstrated good consistency. Phonon densities of states calculated using both finite-displacement method (VASP and PHONOPY[48,49]) and density-functional perturbation theory (QE) showed perfect agreement.

Eliashberg equation[50] was solved to calculate critical temperature T_C. This approach is based on the Fröhlich Hamiltonian

$$\hat{H} = \hat{H}_e + \hat{H}_{ph} + \sum_{k,q,j} g^{q,j}_{k+q,k} \hat{c}^{+}_{k+q} \hat{c}_k (\hat{b}^{+}_{-q,j} + \hat{b}_{q,j})$$

where c^+ and b^+ are creation operators of electrons and phonons, respectively. The QE package was used to calculate matrix elements of electron−phonon interaction $g^{q,j}_{k+q,k}$ in the harmonic approximation as

$$g^{q,j}_{k+q,k} = \sqrt{\frac{\hbar}{2M\omega_{q,j}}} \int \psi^*_k(r) \cdot \left\{ \frac{dV_{scf}}{d\vec{u_q}} \cdot \frac{\vec{u_q}}{|\vec{u_q}|} \right\} \cdot \psi_{k+q}(r)\, d^3r$$

where u_q is the displacement of an atom with mass M in the phonon mode qj. Within the framework of Gor'kov and Migdal approach,[51,52] the correction to the electron Green's function $\Sigma(\vec{k}) = G_0^{-1}(\vec{k}, \omega) - G^{-1}(\vec{k}, \omega)$ caused by the interaction can be calculated by taking into account only the first terms of the expansion of the electron−phonon interaction in ω_{ph}/E_F. As a result, it will lead to integral Eliashberg equations.[50] These equations can be solved by the iterative self-consistent method for the real part of the order parameter $\Delta(T, \omega)$ (superconducting gap) and the renormalization wave function $Z(T, \omega)$[53] (see Supporting Information). We successfully used this approach in our previous work.[31]

In our ab initio calculations of the EPC parameter λ, the first Brillouin zone was sampled using a $6 \times 6 \times 6$ q-point mesh and a denser $24 \times 24 \times 24$ k-point mesh (with Gaussian smearing and $\sigma = 0.025$ Ry, which approximates the zero-width limits in the calculation of λ). In addition to the full solution of Eliashberg equations, more approximate Allen−Dynes and modified McMillan formulas were also used to calculate T_C. The Allen−Dynes formula has the form[54]

$$T_C = \omega_{log} \frac{f_1 f_2}{1.2} \exp\left(\frac{-1.04(1+\lambda)}{\lambda - \mu^* - 0.62\lambda\mu^*} \right) \quad (1)$$

with

$$f_1 f_2 = \sqrt[3]{1 + \left[\frac{\lambda}{2.46(1+3.8\mu^*)} \right]^{3/2}} \cdot \left[1 - \frac{\lambda^2(1-\omega_2/\omega_{log})}{\lambda^2 + 3.312(1+6.3\mu^*)^2} \right] \quad (2)$$

whereas the modified McMillan equation has the form with $f_1 f_2 = 1$.

The EPC constant (λ), logarithmic average frequency (ω_{log}), and mean square frequency (ω_2) as defined as:

$$\lambda = \int_0^{\omega_{max}} \frac{2a^2F(\omega)}{\omega} d\omega \quad (3)$$

and

$$\omega_{log} = \exp\left(\frac{2}{\lambda} \int_0^{\omega_{max}} \frac{d\omega}{\omega} \alpha^2F(\omega) \ln(\omega) \right),$$
$$\omega_2 = \sqrt{\frac{1}{\lambda} \int_0^{\omega_{max}} \left[\frac{2a^2F(\omega)}{\omega} \right] \omega^2 d\omega} \quad (4)$$

and μ^* is the Coulomb pseudopotential, for which we used the widely accepted lower and upper bound values of 0.10 and 0.15, respectively. Calculated critical temperature for Th_4H_{15} at 0 K was found to be 6 K, which nicely agrees with experimental data from refs 11 and 12.

Sommerfeld constant was calculated as:

$$\gamma = \frac{2}{3}\pi^2 k_B{}^2 N(0)(1+\lambda) \quad (5)$$

and was used to estimate the upper critical magnetic field and the superconductive gap in $Fm3m$-ThH_{10} at 100−300 GPa by applying the well-known semiempirical equations of the BCS theory (see eqs 4.1 and 5.11 in ref 55), which work satisfactorily for $T_C/\omega_{log} < 0.25$ (see Table S3):

DOI: 10.1021/acsami.8b17100
ACS Appl. Mater. Interfaces 2018, 10, 43809−43816

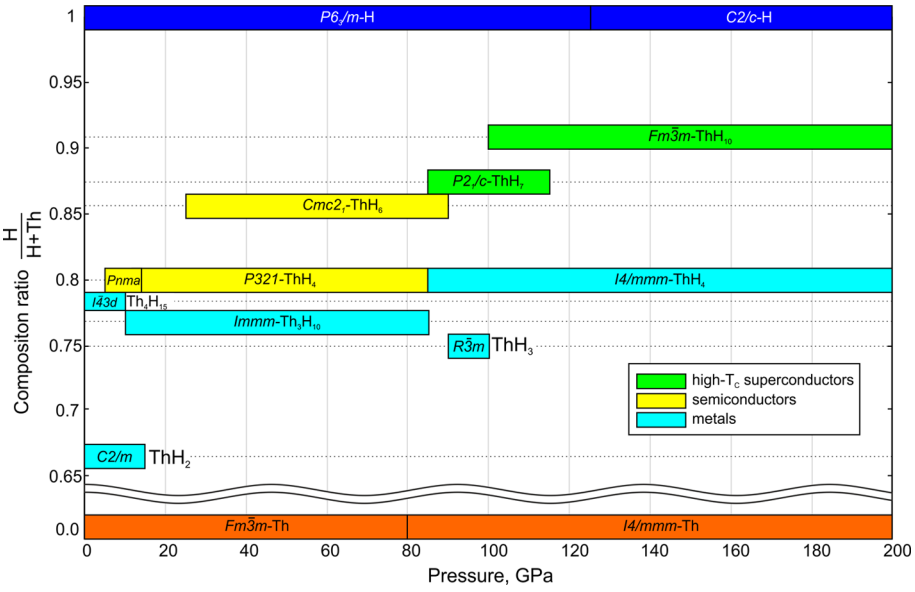

Figure 1. Pressure−composition phase diagram of the Th−H system. Yellow, blue, and green indicate semiconducting, normal metallic, and high-T_C superconducting phases, respectively.

$$\frac{\gamma {T_C}^2}{{H_C}^2(0)} = 0.168\left[1 - 12.2\left(\frac{T_C}{\omega_{log}}\right)^2 \ln\left(\frac{\omega_{log}}{3T_C}\right)\right] \quad (6)$$

$$\frac{2\Delta(0)}{k_B T_C} = 3.53\left[1 + 12.5\left(\frac{T_C}{\omega_{log}}\right)^2 \ln\left(\frac{\omega_{log}}{2T_C}\right)\right] \quad (7)$$

RESULTS

The pressure−composition phase diagram (see Figure 1) was drawn to show pressure ranges of stability of all predicted thorium hydrides. As shown in Figure 1, our calculations correctly reproduce the stability of ThH_2 and Th_4H_{15} and predict eight new stable phases, namely, $R\bar{3}m$-ThH_3, $Immm$-Th_3H_{10}, $Pnma$-ThH_4, $P321$-ThH_4, $I4/mmm$-ThH_4, $Cmc2_1$-ThH_6, $P2_1/c$-ThH_7, and $Fm\bar{3}m$-ThH_{10}.

Detailed information on crystal structures of the predicted phases is summarized in Table S1 (see Supporting Information). It is clearly seen from our calculations that at the pressure of 5 GPa, the new semiconducting $Pnma$-ThH_4 phase becomes stable, whereas increasing pressure leads to a phase transition to semiconducting $P321$-ThH_4 at 15 GPa. Further increase of pressure leads to the $P321 \rightarrow I4/mmm$ phase transition at 85 GPa. At 10 GPa, the $Immm$-Th_3H_{10} phase becomes thermodynamically stable and remains stable up to 85 GPa. The $Cmc2_1$-ThH_6 phase appears on the phase diagram in the pressure range of 25−90 GPa. The $R\bar{3}m$-ThH_3 phase is stable in a narrow pressure range from 90 to 100 GPa. At pressures higher than 100 GPa, only three phases are stable, namely, $I4/mmm$-ThH_4, $P2_1/c$-ThH_7, and $Fm\bar{3}m$-ThH_{10}. Importantly, among the known high-T_C superconducting hydrides, such as LaH_{10},[1] YH_{10},[1] and AcH_{10},[31] thorium decahydride is unique because of its lowest stabilization pressure of 100 GPa, compared to 150 GPa for LaH_{10}[1] (and experimentally synthesized at 170 GPa[32]), 250 GPa for YH_{10},[1] and 200 GPa for AcH_{10}.[31] The $I4/mmm$-ThH_4 and $Fm\bar{3}m$-ThH_{10} phases are stable at least up to 200 GPa, whereas $P2_1/c$-ThH_7 is unstable at pressures above 115 GPa, and at higher pressures only $I4/mmm$-ThH_4 and $Fm\bar{3}m$-ThH_{10} remain thermodynamically and dynamically stable at pressures up to at least 300 GPa.

It is important to note that three of the predicted Th−H phases are semiconductors (yellow color in Figure 1) with the DFT band gaps around 0.6−0.9 eV; note that a systematic underestimation of band gaps by DFT calculations is well-known. The rest of predicted phases $R\bar{3}m$-ThH_3, $Immm$-Th_3H_{10}, $I4/mmm$-ThH_4, $P2_1/c$-ThH_7, and $Fm\bar{3}m$-ThH_{10} are metallic and superconducting. The crystal structure of ThH_{10} is shown in Figure 2. Thorium atoms occupy large 24-

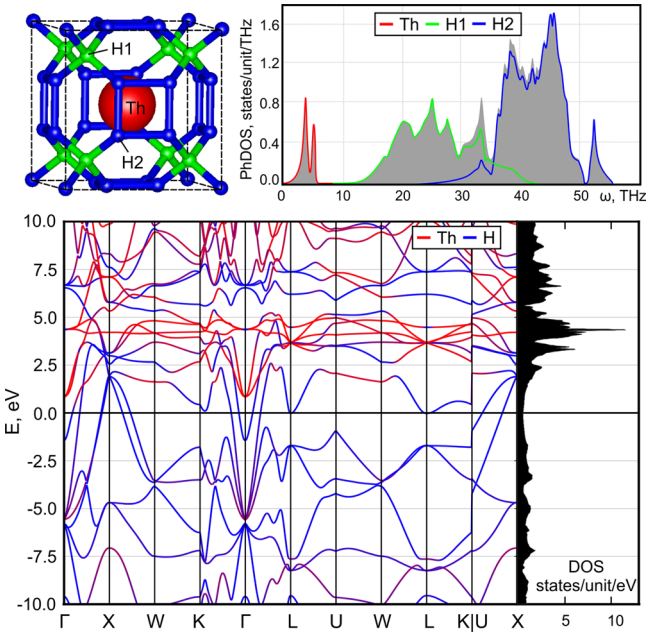

Figure 2. (Top left) Crystal structure, (top right) partial phonon DOS, (bottom) electronic band structure and DOS for predicted $Fm\bar{3}m$-ThH_{10} at 100 GPa. Colors in phonon DOS correspond to colors of atoms in the drawing of the crystal. Crystal structures of predicted phases were visualized using VESTA software.[57]

DOI: 10.1021/acsami.8b17100
ACS Appl. Mater. Interfaces 2018, 10, 43809−43816

Table 1. Predicted Superconducting Properties of Thorium Hydrides

phase	P, GPa	λ	N_f states, A^3 Ry	ω_{log}, K	T_C (McM),[a] K	T_C (A–D),[a] K	T_C (E),[a] K
$R\bar{3}m$-ThH_3	100	0.11	0.42	1664	~0	~0	~0
$Immm$-Th_3H_{10}	10	0.48	0.48	379	3.8 (1.2)	3.9 (1.2)	3.9 (1.2)
$I4/mmm$-ThH_4	85	0.36	0.28	1003	2.97 (0.5)	3.0 (0.5)	3.0 (0.5)
$P2_1/c$-ThH_7	100	0.84	0.23	1192	61.4 (43.4)	64.8 (45.3)	62 (46)
$Fm\bar{3}m$-ThH_{10}	100	2.50	0.215	1073	176.8 (160.3)	221.1 (193.9)	241.2 (220)
	200	1.35	0.227	1627	166.3 (139.4)	182.6 (150.5)	228 (205)
	300	1.11	0.23	1775	144.2 (114.2)	155.4 (121.4)	201 (174)

[a] T_C values are given for $\mu^* = 0.1$, whereas T_C in brackets are for $\mu^* = 0.15$. T_C was calculated using Allen–Dynes (A–D), McMillan (McM) equations, and numerical solution of Eliashberg equation (E).

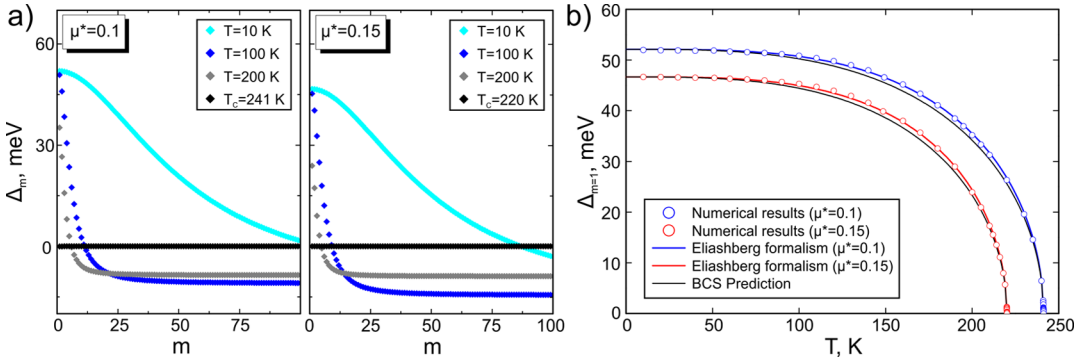

Figure 3. (a) Superconducting order parameter on the imaginary axis for the selected values of temperature calculated at μ^* equals 0.1 and 0.15 for Fm-3m-ThH_{10} at 100 GPa. (b) Temperature dependence of the maximum value of the order parameter. Lines are obtained using eq 8.

coordinated voids in the sodalite-type framework of hydrogens. In $P2_1/c$-ThH_7 each thorium atom has irregular coordination by hydrogen atoms (see Figure S1d in the Supporting Information). Thorium coordination number is remarkably high (23); distances are in the range of 2.03 to 2.23 Å at 100 GPa. We observe high DOS at the Fermi level, which also should be favorable for superconducting properties (see Figure S1d in the Supporting Information).

Phonon calculations confirmed that none of the newly predicted phases have imaginary phonon frequencies in their predicted ranges of thermodynamic stability (see Figure 2 and Figure S1). Calculated partial phonon densities of states of $Fm\bar{3}m$-ThH_{10} show the presence of three major contributions. Two peaks at ~5 THz correspond to vibrations of thorium atoms inside the hydrogen cage. The next sets of peaks (shown in Figure 2, green color) correspond to vibrations of hydrogen atoms located between the hydrogen cubes (H1 type with H–H distance of 1.297 Å). The high-frequency region corresponds to hydrogen atoms in the cubes (H2 type, blue color) with a H–H distance of 1.149 Å. Structures of $R\bar{3}m$-ThH_3, $Immm$-Th_3H_{10}, $I4/mmm$-ThH_4, and $P2_1/c$-ThH_7 phases are shown in Figure S1 (see Supporting Information).

Calculated superconducting properties of thorium hydrides are given in Table 1. The following new phases are metallic and potentially superconducting: $R\bar{3}m$-ThH_3, $Immm$-Th_3H_{10}, $I4/mmm$-ThH_4, $P2_1/c$-ThH_7, and $Fm\bar{3}m$-ThH_{10}. For $Fm\bar{3}m$-ThH_{10} at 100 GPa, the EPC coefficient ($\lambda = 2.50$) and eq 1 as well as numerical solution of the Eliashberg equation were used for calculating T_C. Our calculations indicate that the $\alpha^2F(\omega)$ Eliashberg function of ThH_{10} at 100 GPa has Nb-type behavior with two "hills". For this type of $\alpha^2F(\omega)$ function, the numerical solution of the Eliashberg equations may be approximated by the Allen–Dynes formula, using which we obtained T_c values in the range 194–221 K (depending on the exact μ^* value). Such high values of EPC coefficient and T_C related to vibrations of hydrogen atoms (see Figure 2).

For the most interesting superconducting hydride, $Fm\bar{3}m$-ThH_{10}, accurate numerical solutions of Eliashberg equations were found at pressures 100, 200, and 300 GPa for $\mu^* = 0.1$ and 0.15 (see Table 1 and Supporting Information). In Figure 3a, the form of the order parameter for selected values of temperature (on the imaginary axis) is shown. The superconducting order parameter always takes the largest value for $m = 1$. The maximum value of order parameter decreases when the temperature rises and finally vanishes at the critical temperature (see Figure 3b), and this can be reproduced with the help of the phenomenological formula

$$\Delta_{m=1}(T) = \Delta_{m=1}(T_0)\sqrt{1 - \left(\frac{T}{T_C}\right)^k} \quad (8)$$

where the value of parameter $k = 3.33$ for ThH_{10} was estimated on the basis of the numerical results of $\Delta_{m=1}(T)$. In the framework of BCS theory, parameter k has a constant value, the same for all compounds: $k_{BCS} = 3$.[58]

The high values of the wave function renormalization factor (Z) are related to the significant strong coupling effects. The function of order parameter on the real axis, for selected values of temperature, is presented in Figure S3 (see Supporting Information). It should be noted that the function takes complex values; however, only the real part is nonzero for low frequencies, which means infinite lifetime of Cooper pairs.[58] For higher frequencies, damping effects become significant, which is related to phonon emission and absorption. Complicated dependence of $\mathrm{Re}[\Delta(\omega)]$ and $\mathrm{Im}[\Delta(\omega)]$ for higher frequencies (especially at $T = T_0$) are related to the shape of the Eliashberg function, which has been drawn in Figure S3. Both the real and imaginary parts approach zero at

DOI: 10.1021/acsami.8b17100
ACS Appl. Mater. Interfaces 2018, 10, 43809–43816

the critical temperature, which is related to the disappearance of superconducting properties. From the physical point of view, the most important is the value corresponding to zero frequency, because it specifies the superconducting energy gap and allows one to calculate the value of ratio $R\Delta = 2\Delta(0)/k_BT_C$ (where $\Delta(0) = \mathrm{Re}\,[\Delta(\omega = 0)]_{T = T_0}$), which is a universal constant of BCS theory (3.53, compare with Table 2).

Table 2. Parameters of Superconducting State in $Fm\bar{3}m$-ThH_{10} at 100 GPa

parameter	value ($\mu^* = 0.1$)	value ($\mu^* = 0.15$)
T_C, K	241.2	220.0
$\Delta_{m=1}(T_0)$,[a] meV	52.0	46.7
m_e^*,[c] T_C	$3.63m_e$[b]	$3.73m_e$[b]
$H_C(T_0)$,[a] T	71	64.5
$\Delta C/T_C$, mJ/(mol·K^2)	32.9	32.9
γ,[d] mJ/(mol·K^2)	11.1	11.0
$R_\Delta = 2\Delta(0)/k_BT_C$	5.0	4.9

[a]Here, T_0 = 10 K (initial temperature, below this temperature solutions are not stable). [b]m_e is electron band mass. [c]m_e^* is renormalized electron mass. [d]γ is the Sommerfeld constant.

The free energy difference between the superconducting and normal state has been calculated using the formula[55]

$$\Delta F = -2\pi k_B T N_f \sum_{m=1}^{M} (\sqrt{\omega^2 + \Delta_m^2} - |\omega_m|)\cdot\left(Z_m^S - Z_m^N \frac{|\omega_m|}{\sqrt{\omega^2 + \Delta_m^2}}\right) \quad (9)$$

where Z^S and Z^N are the wave function renormalization factors for superconducting and normal states, respectively, and $N_f = \rho(0)$ is the electronic DOS at the Fermi level.

As a result, the maximum value of the superconducting gap is calculated to be 52 meV (see Table 2, Figure 3, and Table S2), which exceeds that for H_3S (43 meV[59]). This value for ThH_{10} is lower than that for LaH_{10}, YH_{10},[1] and MgH_6.[60] The thermodynamic critical field was computed as $H_c = \sqrt{8\pi(-\Delta F)}$ and equals 64−71 T, which is close to the experimental values for hydrogen sulfide H_3S at 150 GPa (H_C = 60−80 T),[29] but much higher than that for MgB_2 (8 T). A jump in the specific heat at superconducting transition was calculated using $\Delta C(T) = -T \bullet d^2\Delta F/dT^2$ and equals 7.93 J/(mol·K) (see Figure S6 in the Supporting Information).

For $P2_1/c$-ThH_7 at 100 GPa, we find a much lower EPC coefficient of 0.84, resulting in a much lower (but still high) T_C in the range of 46−62 K (see Table 1). At the same time, $R\bar{3}m$-ThH_3 cannot be considered as a superconductor because of the very low EPC coefficient of 0.11 leading to T_C close to 0 K. The calculated T_C of the low-pressure metallic $Immm$-Th_3H_{10} phase is 4 K and is caused by weak electron−phonon interaction (λ = 0.48, ω_{log} = 380 K, see Table 1). The $I4/mmm$-ThH_4 phase shows a low T_C of ∼3 K, along with weak EPC coefficient (λ = 0.36).

It is interesting that metal atoms in the predicted high-temperature superconducting hydrides of lanthanum and yttrium (LaH_{10} and YH_{10}),[1] actinium (AcH_{10}),[31] scandium (ScH_9),[56] and thorium (ThH_{10}) contain almost empty d- and f-shells. Sc, Y, La, and Ac are all d^1-elements; close neighbors of d^0-elements, for example, are $Mg(MgH_6)$[61] and $Ca(CaH_6)$.[62] Now, one can see that a d^2-element (Th) forms the same sodalite-like cubic ThH_{10} and has a remarkably high T_C of ∼241 K. These facts allow us to formulate a rule that d^1- and d^2-metals as well as d^0-metals from II group with a minimal number of f-electrons will be the most promising candidates for discovering high-temperature superconductors.

As $Fm\bar{3}m$-ThH_{10} is stable in a wide range of pressures, we determined the main parameters responsible for superconducting properties as a function of pressure (see Figure 4). We calculated the Eliashberg spectral function $\alpha^2F(\omega)$ as a

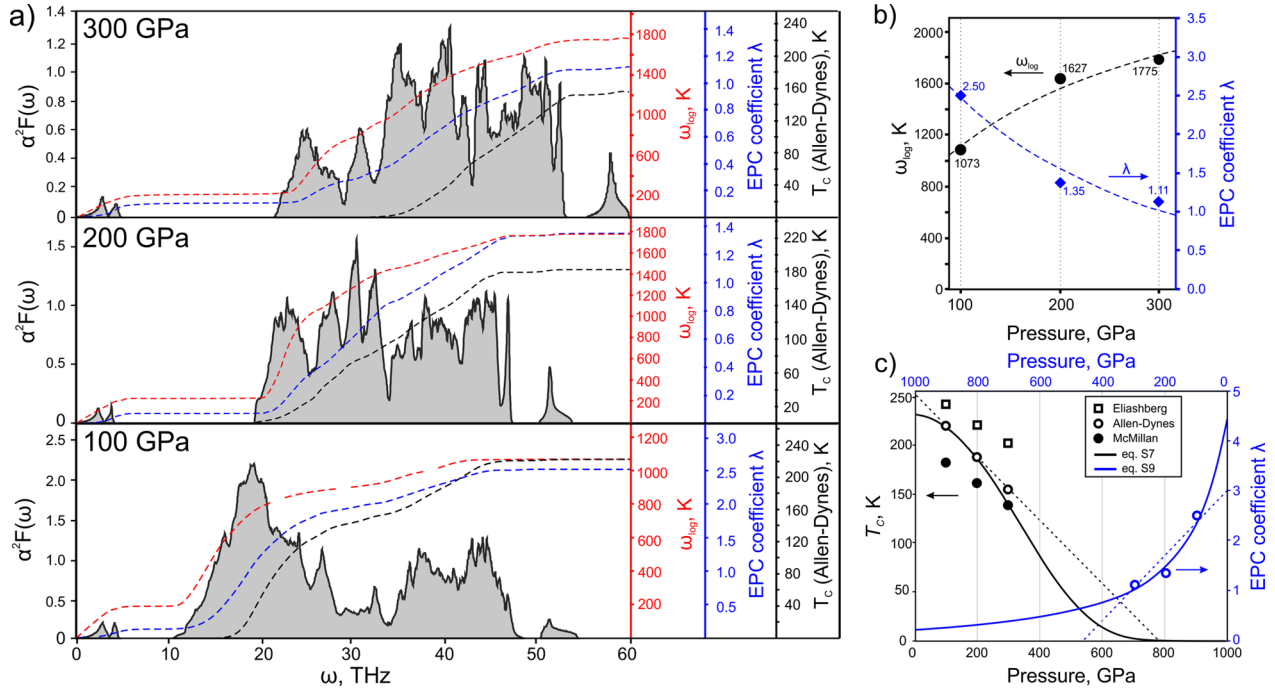

Figure 4. (a) Eliashberg function $\alpha^2F(\omega)$ at pressures from 100 to 300 GPa, (b) ω_{log} and EPC coefficient λ, (c) critical transition temperature (T_C) of $Fm\bar{3}m$-ThH_{10} as a function of pressure.

DOI: 10.1021/acsami.8b17100
ACS Appl. Mater. Interfaces 2018, 10, 43809−43816

function of pressure (see Figure 4a). One can note that increasing pressure leads to shifting of the $\alpha^2F(\omega)$ function to higher frequencies. The EPC coefficient decreases with pressure, whereas ω_{log} increases (see Figure 4b).

It can be seen from Figure 4c, that the dependence of T_C of ThH_{10} on pressure is monotonic and nonlinear and can be described by eq S7. The EPC coefficient calculated using analytical eq S9 also decreases nonlinearly with pressure. These results can be analyzed by the well-known empirical formula for low-T_C superconductors[63,64] $-\ln\left(\frac{T_C}{\omega_{log}}\right) = Cv^{-\varphi}$, $C > 0$, where v is the unit cell volume (see Supporting Information for details). The computed average pressure coefficient $dT_C(E)/dP = -0.20$ K/GPa ($\mu^* = 0.1$) is lower than that for CaH_6 (−0.33 K/GPa).[62]

Theoretically predicted LaH_{10}[1] (with the same structure type as our ThH_{10}) was recently synthesized experimentally,[32] which lends further confidence in structure prediction methods. This material possesses a unique combination of very high T_c and relatively low pressure of synthesis.

CONCLUSIONS

We studied the Th−H system using the global optimization algorithm USPEX to predict new superconducting thorium hydrides, exploring pressures up to 200 GPa. Two new remarkable superconducting polyhydrides were predicted, namely, $Fm\bar{3}m$-ThH_{10} and $P2_1/c$-ThH_7. $Fm\bar{3}m$-ThH_{10} is predicted to be superconducting with T_C in the range of 220−241 K at 100 GPa, a superconducting gap of 47−52 meV, a thermodynamic critical magnetic field of 64−71 T, and a specific heat jump $\Delta C(T_C)/T_C$ equal to 32.9 mJ/(mol·K^2) at 100 GPa. ThH_{10} is one of the highest-T_C superconductors discovered so far. This study completes the investigation of a series of high-T_C superconducting hydrides MgH_6, CaH_6, ScH_9, YH_{10}, LaH_{10}, and AcH_{10}. Thus, a reasonable step after exhausting all promising binary hydrides is to pay more attention to systems of higher complexity, primarily to ternary A−B−H systems.

ASSOCIATED CONTENT

Supporting Information

The Supporting Information is available free of charge on the ACS Publications website at DOI: 10.1021/acsami.8b17100.

Detailed crystal structure of predicted phases, equations for calculations of T_C, detailed description of electronic properties of metallic Th−H phases, Eliashberg spectral functions of superconducting phases, and the dependence of T_C on the pressure for ThH_{10} (PDF)

AUTHOR INFORMATION

Corresponding Authors

*E-mail: A.Kvashnin@skoltech.ru (A.G.K.).
*E-mail: A.Oganov@skoltech.ru (A.R.O.).

ORCID

Alexander G. Kvashnin: 0000-0002-0718-6691

Notes

The authors declare no competing financial interest.

ACKNOWLEDGMENTS

The work was supported by the Russian Science Foundation (No. 16-13-10459). Calculations were performed on the Rurik supercomputer at MIPT and the Arkuda supercomputer of Skolkovo Foundation. A.G.K. thanks the FASIE Foundation for financial support within UMNIK grant No13408GU/2018.

REFERENCES

(1) Liu, H.; Naumov, I. I.; Hoffmann, R.; Ashcroft, N. W.; Hemley, R. J. Potential High-T_c Superconducting Lanthanum and Yttrium Hydrides at High Pressure. *Proc. Natl. Acad. Sci.* **2017**, *114*, 6990−6995.

(2) Drozdov, A. P.; Minkov, V. S.; Besedin, S. P.; Kong, P. P.; Kuzovnikov, M. A.; Knyazev, D. A.; Eremets, M. I. *Superconductivity at 215 K in Lanthanum Hydride at High Pressures*. 2018, arXiv:1808.07039. arXiv.org e-Print archive. https://arxiv.org/abs/1808.07039.

(3) Somayazulu, M.; Ahart, M.; Mishra, A. K.; Geballe, Z. M.; Baldini, M.; Meng, Y.; Struzhkin, V. V.; Hemley, R. J. *Evidence for Superconductivity above 260 K in Lanthanum Superhydride at Megabar Pressures*. 2018, arXiv:1808.07695. arXiv.org e-Print archive. https://arxiv.org/abs/1808.07695.

(4) Cunningham, B. B.; Wallmann, J. C. Crystal Structure and Melting Point of Curium Metal. *J. Inorg. Nucl. Chem.* **1964**, *26*, 271−275.

(5) Griveau, J.-C.; Colineau, É. Superconductivity in Transuranium Elements and Compounds. *C. R. Phys.* **2014**, *15*, 599−615.

(6) Müller, W.; Schenkel, R.; Schmidt, H. E.; Spirlet, J. C.; McElroy, D. L.; Hall, R. O. A.; Mortimer, M. J. The Electrical Resistivity and Specific Heat of Americium Metal. *J. Low Temp. Phys.* **1978**, *30*, 561−578.

(7) Decker, W. R.; Finnemore, D. K. Critical-Field Curves for Gapless Superconductors. *Phys. Rev.* **1968**, *172*, 430−436.

(8) Skriver, H. L.; Mertig, I. Electron-Phonon Coupling of the Actinide Metals. *Phys. Rev. B* **1985**, *32*, 4431−4441.

(9) Allen, P. B. Empirical Electron-Phonon λ Values from Resistivity of Cubic Metallic Elements. *Phys. Rev. B* **1987**, *36*, 2920−2923.

(10) Skriver, H. L.; Eriksson, O.; Mertig, I.; Mrosan, E. Electron-Phonon Coupling in the Actinides. *Phys. Rev. B* **1988**, *37*, 1706−1710.

(11) Dietrich, M.; Gey, W.; Rietschel, H.; Satterthwaite, C. B. Pressure Dependence of the Superconducting Transition Temperature of Th_4H_{15}. *Solid State Commun.* **1974**, *15*, 941−943.

(12) Wickleder, M. S.; Fourest, B.; Dorhout, P. K. Thorium. In *The Chemistry of the Actinide and Transactinide Elements*; Springer: Dordrecht, Netherlands, 2006; pp 52−160, DOI: 10.1007/1-4020-3598-5_3.

(13) Greenwood, N. N.; Earnshaw, A. *Chemistry of the Elements*; Pergamon Press: Oxford, U.K., 1984.

(14) Weaver, J. H.; Knapp, J. A.; Eastman, D. E.; Peterson, D. T.; Satterthwaite, C. B. Electronic Structure of the Thorium Hydrides ThH_2 and Th_4H_{15}. *Phys. Rev. Lett.* **1977**, *39*, 639−642.

(15) Shein, I. R.; Shein, K. I.; Medvedeva, N. I.; Ivanovskii, A. L. Electronic Band Structure of Thorium Hydrides: ThH_2 and Th_4H_{15}. *Phys. B Condens. Matter* **2007**, *389*, 296−301.

(16) Satterthwaite, C. B.; Toepke, I. L. Superconductivity of Hydrides and Deuterides of Thorium. *Phys. Rev. Lett.* **1970**, *25*, 741−743.

(17) Gao, G.; Oganov, A. R.; Bergara, A.; Martinez-Canales, M.; Cui, T.; Iitaka, T.; Ma, Y.; Zou, G. Superconducting High Pressure Phase of Germane. *Phys. Rev. Lett.* **2008**, *101*, 107002.

(18) Gao, G.; Oganov, A. R.; Li, P.; Li, Z.; Wang, H.; Cui, T.; Ma, Y.; Bergara, A.; Lyakhov, A. O.; Iitaka, T.; Zou, G. High-Pressure Crystal Structures and Superconductivity of Stannane (SnH_4). *Proc. Natl. Acad. Sci.* **2010**, *107*, 1317−1320.

(19) Duan, D.; Liu, Y.; Tian, F.; Li, D.; Huang, X.; Zhao, Z.; Yu, H.; Liu, B.; Tian, W.; Cui, T. Pressure-Induced Metallization of Dense $(H_2S)_2H_2$ with High-T_c Superconductivity. *Sci. Rep.* **2014**, *4*, 6968.

(20) Hou, P.; Zhao, X.; Tian, F.; Li, D.; Duan, D.; Zhao, Z.; Chu, B.; Liu, B.; Cui, T. High Pressure Structures and Superconductivity of $AlH_3(H_2)$ Predicted by First Principles. *RSC Adv.* **2015**, *5*, 5096−5101.

DOI: 10.1021/acsami.8b17100
ACS Appl. Mater. Interfaces 2018, 10, 43809−43816

(21) Li, Y.; Hao, J.; Liu, H.; Tse, J. S.; Wang, Y.; Ma, Y. Pressure-Stabilized Superconductive Yttrium Hydrides. *Sci. Rep.* **2015**, *5*, 9948.
(22) Goncharov, A. F.; Lobanov, S. S.; Kruglov, I.; Zhao, X.-M.; Chen, X.-J.; Oganov, A. R.; Konôpková, Z.; Prakapenka, V. B. Hydrogen Sulfide at High Pressure: Change in Stoichiometry. *Phys. Rev. B* **2016**, *93*, 174105.
(23) Esfahani, M. M. D.; Wang, Z.; Oganov, A. R.; Dong, H.; Zhu, Q.; Wang, S.; Rakitin, M. S.; Zhou, X.-F. Superconductivity of Novel Tin Hydrides (Sn_nH_m) under Pressure. *Sci. Rep.* **2016**, *6*, 22873.
(24) Durajski, A. P.; Szczęśniak, R. First-Principles Study of Superconducting Hydrogen Sulfide at Pressure up to 500 GPa. *Sci. Rep.* **2017**, *7*, 4473.
(25) Kruglov, I. A.; Kvashnin, A. G.; Goncharov, A. F.; Oganov, A. R.; Lobanov, S. S.; Holtgrewe, N.; Jiang, S.; Prakapenka, V. B.; Greenberg, E.; Yanilkin, A. V. Uranium Polyhydrides at Moderate Pressures: Prediction, Synthesis, and Expected Superconductivity. *Sci Adv.* **2018**, *4*, eaat9776.
(26) Oganov, A. R.; Glass, C. W. Crystal Structure Prediction Using Ab Initio Evolutionary Techniques: Principles and Applications. *J Chem Phys* **2006**, *124*, 244704.
(27) Oganov, A. R.; Lyakhov, A. O.; Valle, M. How Evolutionary Crystal Structure Prediction Works—and Why. *Acc. Chem. Res.* **2011**, *44*, 227−237.
(28) Lyakhov, A. O.; Oganov, A. R.; Stokes, H. T.; Zhu, Q. New Developments in Evolutionary Structure Prediction Algorithm USPEX. *Comput. Phys. Commun.* **2013**, *184*, 1172−1182.
(29) Drozdov, A. P.; Eremets, M. I.; Troyan, I. A.; Ksenofontov, V.; Shylin, S. I. Conventional Superconductivity at 203 Kelvin at High Pressures in the Sulfur Hydride System. *Nature* **2015**, *525*, 73−76.
(30) Einaga, M.; Sakata, M.; Ishikawa, T.; Shimizu, K.; Eremets, M. I.; Drozdov, A. P.; Troyan, I. A.; Hirao, N.; Ohishi, Y. Crystal Structure of the Superconducting Phase of Sulfur Hydride. *Nat. Phys.* **2016**, *12*, 835−838.
(31) Semenok, D. V.; Kvashnin, A. G.; Kruglov, I. A.; Oganov, A. R. Actinium Hydrides AcH_{10}, AcH_{12}, and AcH_{16} as High-Temperature Conventional Superconductors. *J. Phys. Chem. Lett.* **2018**, *9*, 1920−1926.
(32) Geballe, Z. M.; Liu, H.; Mishra, A. K.; Ahart, M.; Somayazulu, M.; Meng, Y.; Baldini, M.; Hemley, R. J. Synthesis and Stability of Lanthanum Superhydrides. *Angew. Chem. Int. Ed.* **2018**, *57*, 688−692.
(33) Salke, N. P.; Esfahani, M. M. D.; Zhang, Y.; Kruglov, I. A.; Zhou, J.; Wang, Y.; Greenberg, E.; Prakapenka, V. B.; Oganov, A. R.; Lin, J.-F. *Synthesis of Clathrate Cerium Superhydride CeH_9 at 80 GPa with Anomalously Short H-H Distance*. 2018, arXiv:1805.02060, arXiv.org e-Print archive. https://arxiv.org/ftp/arxiv/papers/1805/1805.02060.pdf.
(34) Marizy, A.; Geneste, G.; Loubeyre, P.; Guigue, B.; Garbarino, G. Synthesis of Bulk Chromium Hydrides under Pressure of up to 120 GPa. *Phys. Rev. B* **2018**, *97*, 184103.
(35) Hohenberg, P.; Kohn, W. Inhomogeneous Electron Gas. *Phys Rev* **1964**, *136*, B864−B871.
(36) Kohn, W.; Sham, L. J. Self-Consistent Equations Including Exchange and Correlation Effects. *Phys. Rev.* **1965**, *140*, A1133−A1138.
(37) Perdew, J. P.; Burke, K.; Ernzerhof, M. Generalized Gradient Approximation Made Simple. *Phys. Rev. Lett.* **1996**, *77*, 3865−3868.
(38) Blöchl, P. E. Projector Augmented-Wave Method. *Phys. Rev. B* **1994**, *50*, 17953−17979.
(39) Kresse, G.; Joubert, D. From Ultrasoft Pseudopotentials to the Projector Augmented-Wave Method. *Phys. Rev. B* **1999**, *59*, 1758−1775.
(40) Kresse, G.; Furthmüller, J. Efficient Iterative Schemes for Ab Initio Total-Energy Calculations Using a Plane-Wave Basis Set. *Phys. Rev. B* **1996**, *54*, 11169−11186.
(41) Kresse, G.; Hafner, J. Ab Initio Molecular Dynamics for Liquid Metals. *Phys. Rev. B* **1993**, *47*, 558−561.
(42) Kresse, G.; Hafner, J. Ab Initio Molecular-Dynamics Simulation of the Liquid-Metal Amorphous-Semiconductor Transition in Germanium. *Phys. Rev. B* **1994**, *49*, 14251−14269.
(43) Evans, D. S.; Raynor, G. V. The Lattice Spacing of Thorium, with Reference to Contamination. *J. Nucl. Mater.* **1959**, *1*, 281−288.
(44) Vohra, Y. K.; Akella, J. Thorium: Phase Transformations and Equation of State to 300 GPa. *High Press. Res.* **1992**, *10*, 681−685.
(45) Pickard, C. J.; Needs, R. J. Structure of Phase III of Solid Hydrogen. *Nat. Phys.* **2007**, *3*, 473−476.
(46) Giannozzi, P.; Baroni, S.; Bonini, N.; Calandra, M.; Car, R.; Cavazzoni, C.; Ceresoli, D.; Chiarotti, G. L.; Cococcioni, M.; Dabo, I.; Dal Corso, A.; de Gironcoli, S.; Fabris, S.; Fratesi, G.; Gebauer, R.; Gerstmann, U.; Gougoussis, C.; Kokalj, A.; Lazzeri, M.; Martin-Samos, L.; Marzari, N.; Mauri, F.; Mazzarello, R.; Paolini, S.; Pasquarello, A.; Paulatto, L.; Sbraccia, C.; Scandolo, S.; Sclauzero, G.; Seitsonen, A.P.; Smogunov, A.; Umari, P.; Wentzcovitch, R.M. QUANTUM ESPRESSO: A Modular and Open-Source Software Project for Quantum Simulations of Materials. *J. Phys. Condens. Matter* **2009**, *21*, 395502.
(47) Baroni, S.; de Gironcoli, S.; Dal Corso, A.; Giannozzi, P. Phonons and Related Crystal Properties from Density-Functional Perturbation Theory. *Rev. Mod. Phys.* **2001**, *73*, 515−562.
(48) Togo, A.; Tanaka, I. First Principles Phonon Calculations in Materials Science. *Scr. Mater.* **2015**, *108*, 1−5.
(49) Togo, A.; Oba, F.; Tanaka, I. First-Principles Calculations of the Ferroelastic Transition between Rutile-Type and $CaCl_2$-Type SiO_2 at High Pressures. *Phys. Rev. B* **2008**, *78*, 134106.
(50) Eliashberg, G. M. Interactions between Electrons and Lattice Vibrations in a Superconductor. *J. Exp. Theor. Phys.* **1960**, *11*, 696−702 http://www.jetp.ac.ru/cgi-bin/dn/e_011_03_0696.pdf. .
(51) Gor'kov, L. P. On Energy Spectrum of Superconductors. *J. Exp. Theor. Phys.* **1958**, *34*, 505 http://www.jetp.ac.ru/cgi-bin/dn/e_007_03_0505.pdf. .
(52) Migdal, A. B. Interaction between Electrons and Lattice Vibrations in a Normal Metal. *J. Exp. Theor. Phys.* **1958**, *34*, 996−1001 http://www.jetp.ac.ru/cgi-bin/dn/e_007_06_0996.pdf. .
(53) Maksimov, E. G.; Savrasov, D. Y.; Savrasov, S. Y. The Electron-Phonon Interaction and the Physical Properties of Metals. *Phys.-Usp* **1997**, *40*, 337.
(54) Allen, P. B.; Dynes, R. C. Transition Temperature of Strong-Coupled Superconductors Reanalyzed. *Phys. Rev. B* **1975**, *12*, 905−922.
(55) Carbotte, J. P. Properties of Boson-Exchange Superconductors. *Rev. Mod. Phys.* **1990**, *62*, 1027−1157.
(56) Ye, X.; Zarifi, N.; Zurek, E.; Hoffmann, R.; Ashcroft, N. W. High Hydrides of Scandium under Pressure: Potential Superconductors. *J. Phys. Chem. C* **2018**, *122*, 6298−6309.
(57) Momma, K.; Izumi, F. VESTA 3 for Three-Dimensional Visualization of Crystal, Volumetric and Morphology Data. *J. Appl. Crystallogr.* **2011**, *44*, 1272−1276.
(58) Varelogiannis, G. On the Limits of Consistency of Eliashberg Theory and the Density of States of High-T_c Superconductors. *Z. Phys. B* **1997**, *104*, 411−422.
(59) Durajski, A. P.; Szczęśniak, R.; Pietronero, L. High-Temperature Study of Superconducting Hydrogen and Deuterium Sulfide. *Ann. Phys.* **2016**, *528*, 358−364.
(60) Szczęśniak, R.; Durajski, A. P. Superconductivity Well above Room Temperature in Compressed MgH_6. *Front. Phys.* **2016**, *11*, 117406.
(61) Feng, X.; Zhang, J.; Gao, G.; Liu, H.; Wang, H. Compressed Sodalite-like MgH_6 as a Potential High-Temperature Superconductor. *RSC Adv.* **2015**, *5*, 59292−59296.
(62) Wang, H.; Tse, J. S.; Tanaka, K.; Iitaka, T.; Ma, Y. Superconductive Sodalite-like Clathrate Calcium Hydride at High Pressures. *Proc. Natl. Acad. Sci.* **2012**, *109*, 6463−6466.
(63) Rohrer, H. Druck- und Volumeneffekte in der Supraleitung. *Helv. Phys. Acta* **1960**, *33*, 675−705.
(64) Olsen, J. L.; Rohrer, H. The volume dependence of the electron level density and the critical temperature in superconductors. *Helv. Phys. Acta* **1960**, *33*, 872−880.

DOI: 10.1021/acsami.8b17100
ACS Appl. Mater. Interfaces 2018, 10, 43809−43816

NOTE ADDED AFTER ASAP PUBLICATION

This paper was published on the Web on December 4, 2018. Additional text corrections were added to the paper, and the corrected version was reposted on December 7, 2018.

DOI: 10.1021/acsami.8b17100
ACS Appl. Mater. Interfaces 2018, 10, 43809−43816